HHS Public Access

Author manuscript

Dev Biol. Author manuscript; available in PMC 2017 August 28.

Published in final edited form as:

Dev Biol. 2016 August 01; 416(1): 111–122. doi:10.1016/j.ydbio.2016.05.038.

Genetic and biochemical evidence that gastrulation defects in *Pofut2* mutants result from defects in ADAMTS9 secretion

Brian A. Benz[a], **Sumeda Nandadasa**[b], **Megumi Takeuchi**[c], **Richard C. Grady**[a], **Hideyuki Takeuchi**[c], **Rachel K. LoPilato**[c], **Shinako Kakuda**[a], **Robert P.T. Somerville**[b], **Suneel S. Apte**[b], **Robert S. Haltiwanger**[c,*], and **Bernadette C. Holdener**[a,*]

[a]Department of Biochemistry and Cell Biology, Stony Brook University, Stony Brook, NY, United States

[b]Department of Biomedical Engineering, Cleveland Clinic Lerner Research Institute, Cleveland, OH, United States

[c]Complex Carbohydrate Research Center, University of Georgia, Athens, GA 30602, United States

Abstract

Protein *O*-fucosyltransferase 2 (POFUT2) adds *O*-linked fucose to Thrombospondin Type 1 Repeats (TSR) in 49 potential target proteins. Nearly half the POFUT2 targets belong to the A Disintegrin and Metalloprotease with ThromboSpondin type-1 motifs (ADAMTS) or ADAMTS-like family of proteins. Both the mouse *Pofut2 RST434* gene trap allele and the *Adamts9* knockout were reported to result in early embryonic lethality, suggesting that defects in *Pofut2* mutant embryos could result from loss of *O*-fucosylation on ADAMTS9. To address this question, we compared the *Pofut2* and *Adamts9* knockout phenotypes and used Cre-mediated deletion of *Pofut2* and *Adamts9* to dissect the tissue-specific role of *O*-fucosylated ADAMTS9 during gastrulation. Disruption of *Pofut2* using the knockout (*LoxP*) or gene trap (*RST434*) allele, as well as deletion of *Adamts9,* resulted in disorganized epithelia (epiblast, extraembryonic ectoderm, and visceral endoderm) and blocked mesoderm formation during gastrulation. The similarity between *Pofut2* and *Adamts9* mutants suggested that disruption of ADAMTS9 function could be responsible for the gastrulation defects observed in *Pofut2* mutants. Consistent with this prediction, CRISPR/Cas9 knockout of *POFUT2* in HEK293T cells blocked secretion of ADAMTS9. We determined that *Adamts9* was dynamically expressed during mouse gastrulation by trophoblast giant cells, parietal endoderm, the most proximal visceral endoderm adjacent to the ectoplacental cone, extraembryonic mesoderm, and anterior primitive streak. Conditional deletion of either *Pofut2* or *Adamts9* in the epiblast rescues the gastrulation defects, and identified a new role for *O*-fucosylated ADAMTS9 during morphogenesis of the amnion and axial mesendoderm. Combined, these results suggested that loss of ADAMTS9 function in the extra embryonic tissue is responsible for gastrulation defects in the *Pofut2* knockout. We hypothesize that loss of ADAMTS9 function in the most proximal visceral endoderm leads to slippage of the visceral endoderm and altered characteristics of the extraembryonic ectoderm. Consequently, loss of input from the extraembryonic ectoderm and/or compression of the epiblast by Reichert's membrane

*Corresponding authors. rhalti@uga.edu (R.S. Haltiwanger), bernadette.holdener@stonybrook.edu (B.C. Holdener).

blocks gastrulation. In the future, the *Pofut2* and *Adamts9* knockouts will be valuable tools for understanding how local changes in the properties of the extracellular matrix influence the organization of tissues during mammalian development.

Keywords

O-Fucosylation; *Pofut2*; *Adamts9*; Thrombospondin type I repeats; Gastrulation

1. Introduction

Thrombospondin Type I Repeats (TSRs) are small (40–60 a.a.) protein motifs found in multiple secreted and cell-surface proteins that participate in diverse cellular activities including cell attachment, extracellular matrix (ECM) remodeling, migration, proliferation, and apoptosis (Adams and Tucker, 2000). Many TSR-containing proteins require post-translational modification with an unusual disaccharide, Glucoseβ1-3Fucose, for proper localization and function (Niwa et al., 2015; Ricketts et al., 2007; Vasudevan et al., 2015; Wang et al., 2007). This disaccharide is added only to properly folded TSRs containing an *O*-fucose consensus sequence (C-X-X-(S/T)-C) through the sequential action of Protein *O*-FUcosylTransferase 2 (POFUT2) and β3-GLuCosyl-Transferase (B3GLCT) (Kozma et al., 2006; Luo et al., 2006; Sato et al., 2006; Valero-Gonzalez et al., 2016). Loss of POFUT2 impairs secretion of target proteins and causes severe gastrulation defects in mouse embryos (Du et al., 2010; Vasudevan et al., 2015). In contrast, only some targets appear sensitive to B3GLCT elimination (Vasudevan et al., 2015), and mutations in human *B3GLCT,* rather than resulting in early embryo lethality similar to the mouse *Pofut2* mutants, cause Peters Plus Syndrome (PPS), a congenital disorder characterized by Peters anomaly of the eye (congenital corneal opacity arising from a persistent lens stalk), broadened facial features, brachydactyly, shortened limbs, and developmental delay (Lesnik Oberstein et al., 2006).

POFUT2 is predicted to modify forty-nine targets, including members of Thrombospondin, ADAMTS (A Disintegrin and Metalloprotease with Thrombospondin Type 1 Repeats) and ADAMTS-like (ADAMTSL), CCN (named for its members Cyr61, CTGF, and Nov), and BAI (Brain-specific Angiogenesis Inhibitor) families, and several other proteins that interact with the ECM (Du et al., 2010). About half the predicted targets are members of the ADAMTS super-family. The secreted ADAMTS proteases cleave a variety of ECM substrates and have important roles in modulating the structure and function of the ECM components and other secreted molecules (Apte, 2009; Dubail and Apte, 2015). ADAMTSLs resemble the C-terminal ancillary domain of ADAMTS proteases but lack a protease domain (Apte, 2009). Several ADAMTSLs bind to fibrillins, which form tissue microfibrils that provide important mechanical ECM properties and regulate BMP and TGFβ signaling (Hubmacher and Apte, 2011). Mutations in mouse and human ADAMTS and ADAMTSL proteins lead to a variety of developmental defects and inherited connective tissue disorders (Dubail and Apte, 2015).

In this study, we used conditional deletion of *Pofut2* during early mouse development to demonstrate that defects in the extraembryonic tissues contribute to abnormal epithelial

organization in *Pofut2* mutants. Through analysis of *Adamts9* mRNA localization and comparison of *Pofut2* mutants with *Adamts9* null and conditional deletion mutants, we identified ADAMTS9 as the likely POFUT2 target responsible for maintaining normal epithelia arrangement and early gastrulation. Cell-based assays with *POFUT2*-deleted cells revealed that *O*-fucosylation is required for proper secretion of ADAMTS9, suggesting that localized defects in the organization or properties of the ECM were likely responsible for the *Pofut2* and *Adamts9* mutant phenotypes. Analysis of the *Pofut2* and *Adamts9* conditional epiblast mutants also identified a role for POFUT2 during axis formation. The abnormalities in these mutants suggest a role for POFUT2 targets including ADAMTS9 in morphogenesis of the amnion and axial mesendoderm.

2. Materials and methods

2.1. Ethics statement

All animal work was conducted according to relevant national and international guidelines and under approved protocols at Stony Brook University and the Cleveland Clinic under Assurance #3145-01. Stony Brook University operates under Assurance #A3011-01, approved by the NIH Office of Laboratory Animal Welfare (OLAW). The animal studies were approved by the Institutional Animal Care and Use and Committee (IACUC) which follow all the guidance set forth in: Public Health Service Policy on Humane Care and Use of Laboratory Animals distributed by Office of Laboratory Animal Welfare, NIH; Animal Welfare Act and Animal Welfare Regulations distributed by United States Department of Agriculture; and Guide for the Care and Use of Laboratory Animals distributed by the National Research Council. Stony Brook University animal facilities are accredited with AAALAC International (Association for the Assessment and Accreditation of Laboratory Animal Care International).

2.2. Mice and genotyping

Primers used and conditions for genotyping are listed in Supplementary Table 1, and maps of *Pofut2* alleles are depicted in Supplementary Fig. 1. The *Pofut2*$^{Gt(RST434)Byg}$ (*Pofut2-RST434*) transgenic mice were previously described, and have subsequently been backcrossed 23 generations to C57BL/6J (Du et al., 2010). The *Pofut2*^{tm1bch} allele (*Pofut2-Floxed+Neo*) was generated by *Ozgene*. The targeting construct was electroporated into the C57BL/6 embryonic stem (ES) cell line, Bruce4. Homologous recombinant ES cells were injected into blastocysts from C57BL/6-albino mice, which were congenic for the *Tyr<c-Brd>* mutation on the C57BL/6Ncr genetic background. Chimeras were mated to C57BL/6J and subsequent progeny were backcrossed to C57BL/6J. Embryos homozygous for the *Pofut2-Floxed+Neo* allele were not viable. To remove the *Neo*-cassette and generate the *Pofut2*$^{tm2.1bch}$ floxed allele (*Pofut2-Floxed*), *Pofut2-Floxed+Neo* heterozygotes were crossed to animals that ubiquitously express Flp recombinase (B6.129S4-*Gt(ROSA)26Sor*$^{tm1(FLP1)Dym}$/RainJ). *Pofut2-Floxed* heterozygotes were backcrossed to C57BL/6J for 5 generations and were then maintained by intercross. To generate the *Pofut2*$^{tm2.2bch}$ knockout allele (*Pofut2-LoxP*), *Pofut2-Floxed* heterozygotes were mated to PGK-Cre-recombinase expressing mice obtained from Ozgene (C57BL/6 background) (Taibi et al., 2013) and were then maintained by backcrossing to C57BL/6J for 6

generations. The *Adamts9*$^{tm1.2Apte}$ knockout (*Adamts9-del)* and Floxed (*Adamts9-Floxed*) alleles were previously described (Dubail et al., 2014). *Adamts9-del* and *Adamts9-Floxed* were subsequently maintained by backcrossing to C57BL/6J. *Adamts9*^{tm1Dgen} (*Adamts9-LacZ*) allele containing an IRES-lacZ cassette in exon 12 (TSR1) was previously described (McCulloch et al., 2009). Timed pregnancies were obtained for these studies by designating the morning of observation of a vaginal plug as embryo age (E) 0.5.

2.3. Whole-mount embryo in situ hybridization, β-galactosidase staining, and histology

For histology, deciduae were isolated at embryonic day (E) 7.5, fixed in 4% paraformaldehyde (PFA), embedded in paraffin, sectioned and stained with hematoxylin and eosin. *In situ* hybridization was carried out as previously described in Shumacher et al. (1996), with the addition of an RNAse step for the *Lefty2* probe. To reduce trapping in *Pofut2* mutant embryos, tissues were perforated with a tungsten needle. DNA constructs for probe preparation were kindly provided by Drs. Brigid Hogan (*Bmp4*), Janet Rossant (*Kdr* (*Flk1*)), Elizabeth Lacy (*Foxa2*), Michael M Shen (*Lefty2*), Thomas Gridley (*Snail*), and Bernhard Herrman (*T*). The *Adamts9* probe was previously described (Jungers et al., 2005). Embryos subjected to *in situ* hybridization (ISH) were fixed in 4% PFA, rinsed in PBS, and cleared in 80% glycerol before photographing on an agarose background. Photographs were taken on a Zeiss SteREO microscope using an AxioCam MRc camera and AxioVisionLE program. To genotype embryos that were processed for *in situ*, the embryos were rehydrated in PBS and lysed in 25–50 μl PCR buffer containing (200 mg/mL proteinase K, 10 mM DTT, 50 mM KCl, 1.5 mM $MgCl_2$, 10 mM Tris HCl pH8.5, 0.01% gelatin, 0.45% NP-40, 0.45% Tween-20). Embryo lysates were heated to 95 °C for 10 min and 0.1–2 μl were used directly for PCR as described in Supplementary Table 1. Primers and conditions used for genotyping are listed in Supplementary Table 1 and the locations of primers within the *Pofut2* gene are shown in Supplementary Fig. 1. β-galactosidase staining of embryos was done as previously described (McCulloch et al., 2009).

2.4. RT-PCR analysis

To examine expression of *Pofut2* alleles, RNA was isolated from pooled E 8.5 embryos obtained from a *Pofut2-RST434/+* X C57BL/6J cross. Total RNA was isolated using the RNAqueous Micro Total RNA isolation kit from Life Technologies. RT-PCR was performed using the SuperScript III One-Step RT-PCR System with Platinum Taq DNA polymerase kit from Life Technologies and the primers indicated in Supplementary Fig. 2.

2.5. Cell-based ADAMTS9 secretion assays

2.5.1. Generation of POFUT2 CRISPR/Cas9 POFUT2 knockout HEK293T cells

—POFUT2 knockout HEK293T cells were generated using CRISPR/Cas9 knockout plasmids from SantaCruz. The *POFUT2* knockout plasmids contained a pool of three plasmids each encoding the Cas9 nuclease/GFP and a *POFUT2*-specific guide RNA (gRNA). The sequences of the three gRNAs are 5′-CGTCCTGCAAAGTTACGCAG-3′, 5′-TGTAGTACTCGTGCTTGTCC-3′, and 5′-CTCTGCTGAAGACGGAGGAG-3′. Semi-confluent (60–80%) HEK293T cells in a 6-well dish were transfected with 2 μg of control or POFUT2-specific KO plasmids using 10 μl of UltraCruz transfection reagent according to

the manufacturer's protocol. After overnight culture, single GFP-positive cells were sorted in 96-well plates using the MoFlo XDP Cell Sorter (Beckman Coulter) at the CTEGD Cytometry Shared Resource Laboratory at the University of Georgia (http://ctegdcytometry.ovpr.uga.edu). Successful gene targeting was confirmed by genomic PCR and Western blot analysis (data not shown). For genomic PCR, we used Herculase Enhanced polymerase (Agilent Technology) and the following primer sets: 5′-GAAACCTCAGCATTTGAGACCT-3′ and 5′-GAACTGCTCATACTCG ATGACG-3′; 5′-ACTTCACCTTCGCGATGCTC-3′ and 5′-GGTAGTGTCAGAGCCTTTAATGGC-3′. POFUT2 polyclonal antibody was from Proteintech, catalog no. 17764-1-AP.

2.5.2. Secretion assay—Wild-type HEK293T and *Pofut2* knockout HEK293T cells were plated in 12 well plates and grown to 70–80% confluency in DMEM (Invitrogen) with 10% bovine calf serum. Cells were transfected using polyethylenimine (PE) (Thomas et al., 2005) as the transfection reagent with a total of 0.82 μg of DNA (0.6 μg ADAMTS9-N-L2 or pSecTag2 empty vector, 0.12 μg mPOFUT2 or pcDNA4 empty vector, and 0.1 μg hIgG). The pSecTag2 and pcDNA4 vectors in the study were purchased from Invitrogen (Thousand Oaks, CA). The hIgG and ADAMTS9-N-L2 constructs were previously described (Hsieh et al., 2003; Koo et al., 2010). After 4 h, the medium was removed and replaced with 0.4 mL of OptiMEM (Invitrogen). Following a 48 h incubation period, media was collected and cells were lysed using 0.4 mL lysis buffer (TBS with 1% glycerol and 1% NP-40) containing cOmplete Mini, EDTA-free protease inhibitor (Roche). Media and lysate samples were separated using 8% SDS-PAGE. Protein was transferred to a 0.45 μm nitrocellulose membrane, rinsed in Phosphate Buffered Saline (PBS) with 0.1% Tween-20 (PBST), and blocked with 5% dry milk in PBST for one hour at room temperature before adding a 1:2000 dilution of anti-myc antibody (9E10, Stony Brook University Cell Culture/Hybridoma Facility) in blocking solution (5% dry milk in PBST) overnight at 4 degrees. The membrane was washed with PBST before adding a 1:10,000 dilution of the anti-mouse Alexafluor680 (Life Technologies) secondary antibody and IRDye800 anti-human IgG (Rockland Immunochemicals) and incubating for one hour. Before imaging, membranes were washed 3 times with PBST and 2 times with deionized water. The membrane was imaged using the Odyssey CLx and analyzed with Image Studio Lite software (LI-COR Biosciences).

3. Results

3.1. Pofut2 knockout blocks gastrulation

Previously, we characterized the effects of the *Pofut2-RST434* gene trap insertion on mouse embryo development (Du et al., 2010). This gene trap likely generated a null allele since the insertion of the gene trap cassette was predicted to result in a fusion protein that lacked the catalytic residues from POFUT2 (Chen et al., 2012 and Supplementary Fig. 1). Gastrulation was severely affected in *Pofut2-RST434* mutants (Du et al., 2010). Reichert's membrane was highly compressed and the epithelia of the visceral endoderm, extraembryonic ectoderm and the epiblast were irregular. In addition, epithelial to mesenchymal transition was significantly expanded in the primitive streak. It was unclear whether gastrulation defects observed in these mutants occurred secondarily to the highly compressed Reichert's membrane observed in the mutants. To begin to address this question, we developed another

Pofut2 allele that would be suitable for conditional deletion analyses (*Pofut2-Floxed*), and used Cre-recombinase to generate the *Pofut2* knockout allele (*Pofut2-LoxP*) (Supplementary Fig. 1).

To confirm that the *Pofut2-LoxP* allele was null, we compared progeny from *Pofut2-LoxP/+* intercrosses using inspection of whole embryos, hematoxylin and eosin staining of sectioned embryos, and *in situ* hybridization to examine markers of extraembryonic ectoderm and mesoderm differentiation (Fig. 1). At E 6.5 *Pofut2-LoxP* mutants were morphologically indistinguishable from wild-type littermates, suggesting a normal arrangement of embryonic and extraembryonic tissues (not shown). At E 7.5, wild-type embryos had reached the mid to late primitive streak stage (Downs and Davies, 1993) (Fig. 1A–B′). In intact and sectioned wild-type embryos, the embryonic and extraembryonic mesoderm was visible, and the extraembryonic amnion and chorion were forming (Fig. 1A–B′). Apical vacuoles were clearly visible in the proximal visceral endoderm (Fig. 1B′). In contrast, the *Pofut2-LoxP* mutant embryos were shorter and rounder in appearance, lacked mesoderm, had thickened visceral endoderm, and appeared constricted proximal to the epiblast (Fig. 1C–D′), similar to what we previously described in the *Pofut2-RST434* mutants (Du et al., 2010). The embryonic and extraembryonic epithelia were also irregular in *Pofut2-LoxP* mutants, and apical vacuoles were absent from the proximal visceral endoderm (Fig. 1D, D′). The correct localization of anterior visceral endoderm (AVE) markers in *Pofut2-RST434* mutants (Du et al., 2010), suggests that failure of the distal visceral endoderm (DVE) cells to move to the anterior does not explain the observed thickened distal visceral endoderm. Rather, the increased laminin staining observed in *Pofut2-RST434* Reichert's membrane (Du et al., 2010), raised the possibility that altered characteristics of this membrane compress the embryo and may restrict the physical expansion of the visceral endoderm. Continued cell proliferation within in a restricted environment would lead to the thickened appearance of the visceral endoderm and disorganization of the epiblast. By E 9.5 *Pofut2-LoxP* mutants were resorbed.

Consistent with the lack of visible mesoderm in *Pofut2-LoxP* mutant embryos, *Snail,* normally expressed in the migrating mesoderm in wild-type embryos (Fig. 1E, left), was only significantly expressed in one of four *Pofut2-LoxP* mutants (Fig. 1E, right). Similarly, *Flk1,* normally expressed in the extraembryonic mesoderm of wild-type embryos (Fig. 1F, left) was absent in four out of eight embryos (not shown), showed limited expression in three out of eight embryos, and showed strong expression in only one embryo (Fig. 1F, right). *Bmp4* was expressed in the extraembryonic ectoderm of wild-type embryos at E 6.5 and in the extraembryonic mesoderm at E 7.5 (Fig. 1G and H, respectively). In contrast, *Bmp4* was not detected in *Pofut2-LoxP* mutants (Fig. 1G and H). The absence of *Bmp4* expression in *Pofut2-LoxP* mutants suggests that the characteristics of the extraembryonic ectoderm may be altered.

Overall, the appearance of the *Pofut2-LoxP* mutants and disorganization of epithelia were similar to what we observed for the *Pofut2-RST434* mutants. However, the lack of mesoderm differentiation and limited expression of *Snail* and *Flk1* in *Pofut2-LoxP* mutants contrasted markedly with our previous observation that the *Pofut2-RST434* gene trap insertion resulted in abundant *Flk1* and *Snail* expression and excessive epithelial to

mesenchymal transition (EMT) in the epiblast (Du et al., 2010). We hypothesized that the distinct phenotypes could result from either partial function of the *Pofut2-RST434* allele through alternative splicing or from the influence of differences in genetic background. The *Pofut2-RST434* gene trap insertion disrupted *Pofut2* exon 6 (Supplemental Fig. 1; Du et al., 2010), and hypothetical alternative splicing between exon 5 and 7 could maintain the POFUT2 reading frame. For this reason, we used RT-PCR to determine whether alternatively spliced transcripts originate from the *Pofut2-RST434* allele (Supplementary Fig. 2). We detected RT-PCR products specific for transcripts originating from the *Pofut2* wild-type and the *Pofut2-RST434* allele. We did not detect a product that would result from alternative splicing between exons 5 and 7, demonstrating that phenotypic differences between Du et al. (2010) and this study did not result from an alternatively spliced hypomorphic *Pofut2-RST434* allele.

Since the previous study (Du et al., 2010), we had extensively backcrossed the *Pofut2-RST434* allele to C57BL/6J 23 generations and fixed the C57BL/6J Y chromosome in the *Pofut2-RST434* background. For this reason, we re-examined the expression of *Snail* and *Bmp4* in *Pofut2-RST434* mutants (Fig. 1I and J). In contrast to our previous studies, we failed to detect mesodermal *Snail* expression in three *Pofut2-RST434* mutants, although *Snail* was expressed in the trophectoderm (Fig. 1I). At E 7.5, expression of Bmp4 was barely detectable in two *Pofut2-RST434* mutants, and the position of the signal suggested that extraembryonic ectoderm could be displaced in the *Pofut2* mutant (Fig. 1J). The similarity between the *Pofut2-LoxP* and *Pofut2-RST434* alleles provided strong evidence that these alleles were null and that *Pofut2* was required to maintain the organization of epithelia in the early gastrula. For this reason, we hypothesize that the phenotypic differences between the Du study (Du et al., 2010) and the current resulted from differences in genetic background.

3.2. Pofut2 activity in the extraembryonic tissues is essential for gastrulation

To determine whether loss of mesoderm in *Pofut2* mutants resulted from defects in the epiblast, or rather occurs secondarily to defects in the extraembryonic tissues, we examined the effects of Sox2::Cre mediated deletion of *Pofut2* in the epiblast on gastrulation (hereafter referred to as *Pofut2* epiblast mutant) (Fig. 2 and Supplementary Fig. 3). At E 7.5, both wild-type and *Pofut2* epiblast mutant embryos underwent gastrulation and extraembryonic membranes were visible, including the amnion, chorion, and allantois (Fig. 2A, B, and G). Frequently in the *Pofut2* epiblast mutants, the closure of the proamniotic cavity appeared delayed or the chorion remained connected to the amnion (Fig. 2B and G, right, asterisk). Consistent with the ability of *Pofut2* epiblast mutants to undergo gastrulation, E 7.5 *Pofut2* epiblast mutants expressed *T* in the notochord and head process and *Foxa2* in the anterior primitive streak and emerging mesendoderm, similar to that seen in wild-type littermates (Fig. 2A and B). However in *Pofut2* epiblast mutants, the *Foxa2* expressing cells located anterior to the primitive streak appeared to be more widely dispersed along the midline (Fig. 2B). Overall, the normal epithelial arrangement and progression of gastrulation in *Pofut2* epiblast mutants provided strong evidence that the block in gastrulation in the *Pofut2* knockout was secondary to defects in the extraembryonic tissue.

3.3. POFUT2 activity in epiblast-derived cells is important for morphogenesis of the extraembryonic membranes and axis elongation

By E 8.5 the morphology of the *Pofut2* epiblast mutant embryos could be clearly distinguished from wild-type littermates by their characteristic shortened and kinked axis, failure to turn, and irregular extraembryonic membranes (Fig. 2C–F and H right). Although they were abnormal, headfold, heart, and somites were present in *Pofut2* epiblast mutants (Fig. 2E, F and H, right). Abnormal attachments between the chorion and amnion persisted in the *Pofut2* epiblast mutants (Fig. 2D, right). *T* was expressed at Theiler stage 12 and 14 in the primitive streak and condensed notochord in wild-type littermates (Fig. 2C and E, left). *Foxa2* was similarly expressed in the notochord at the early headfold stage and also observed in the notochord and floorplate by Theiler stage 14 (Fig. 2D and F, left). Expression of *T* and *Foxa2* in the midline of *Pofut2* epiblast mutants provided evidence that axial mesoderm was specified. However, the broadened midline expression of *T* and *Foxa2* in the posterior notochord and discontinuous expression of *T* in later *Pofut2* epiblast littermates (Fig. 2C–F, right) suggested that *Pofut2* activity in epiblast-derived cells was needed for efficient midline convergence of the anterior head process or convergent extension movements in the trunk notochord precursors (Poelmann, 1981; Sulik et al., 1994; Yamanaka et al., 2007). Combined, these analyses point to the importance of *O*-fucosylation of POFUT2 targets in epiblast derived cells for morphogenesis of the extraembryonic membranes and axis elongation.

3.4. Definitive endoderm intercalates in Pofut2 epiblast mutants

Expression of *Foxa2* in E 7.5 *Pofut2* epiblast mutants provided evidence that the definitive endoderm cells are specified. *Foxa2* expressing cells normally intercalate into the overlying visceral endoderm, to form the definitive endoderm (Kwon et al., 2008). To provide a preliminary assessment of whether the definitive endoderm cells intercalated into the visceral endoderm layer in *Pofut2* epiblast mutants, we used PCR to determine whether the wild-type *Pofut2-Floxed/RST434* visceral endoderm cells were depleted in the E 8.5 *Pofut2* epiblast mutants (Fig. 2E inset, Supplementary Fig. 3, and data not shown). In the *Pofut2-Floxed/Pofut2-LoxP;Sox2::Cre* wild-type E 8.5 embryos (n = 6), the *Pofut2-wt* and *Pofut2-LoxP* alleles predominated, with barely perceptible *Pofut2-floxed* allele. This result is consistent with the significant contribution of the epiblast cells to the definitive endoderm. Similar results were obtained in *Pofut2-floxed/Pofut2-RST434;Sox2::Cre* embryos (n = 11), where the *Pofut2-LoxP* and *Pofut2-RST434* alleles dominated. These results provided evidence that the *Pofut2* mutant epiblast cells could disperse and intercalate into the surface visceral endoderm layer to form the definitive endoderm, but did not exclude the possibility that altered properties of the definitive endoderm layer also contribute to the axis elongation defects observed in *Pofut2* epiblast mutant embryos.

3.5. Pofut2 epiblast mutants likely generate a leftward-directed nodal signal

Since the trunk notochord is derived from the node, the expression of *T* and *Foxa2* in the *Pofut2* epiblast mutants (Fig. 2) provided indirect evidence that the node had assembled in *Pofut2* epiblast mutants (Kinder et al., 2001; Lee and Anderson, 2008; Sulik et al., 1994; Yamanaka et al., 2007). However, since *Pofut2* was essential for maintaining epithelial

organization in the gastrula, we wanted to determine whether loss of *Pofut2* in the epiblast disrupted the node organization. Generally, mutations that disrupt node epithelial organization, such as mutations in planar cell polarity genes or the gene encoding the FERM domain protein Lulu, interfere with establishment of left/right laterality (Lee et al., 2010; Montcouquiol et al., 2003; Wang et al., 2006). As a first step towards determining whether loss of *Pofut2* interferes with organization of the node, we evaluated the expression of *Lefty2* in the left lateral plate mesoderm (Fig. 3A). *Lefty2* is normally transiently activated in the lateral plate mesoderm in response to the leftward flow of Nodal signal (Shiratori and Hamada, 2006). At E 7.5, *Lefty2* was similarly expressed in wild-type and *Pofut2* epiblast mutants in the wings of mesoderm leaving the primitive streak (not shown).

By E 8.5, *Lefty2* was expressed in 5 of the 12 wild-type litter-mates, consistent with the transient activation of *Lefty2* in the left lateral plate mesoderm (Fig. 3A). *Lefty2* was expressed to varying degrees in the left lateral plate mesoderm of the majority of *Pofut2* epiblast mutants (n = 15/23) (Fig. 3B–E). Although compressed in size relative to their wild-type counterparts, the *Pofut2* epiblast mutant embryos are undergoing similar developmental processes (neural folds, heart, and somites forming) but are slightly delayed, and for this reason we predict that the minority of mutants that did not express *Lefty2* had down regulated *Lefty2* similar to the majority of wild-type littermates. Mouse mutations that disrupt the leftward flow of NODAL express *Lefty2* either bilaterally or not at all (Basu and Brueckner, 2008; Lee and Anderson, 2008). For this reason the left sided localization *of Lefty2*, and absence of mutants with expression on both sides, suggests that the node cilia are functional in *Pofut2* epiblast mutants. However, because as few as two beating cilia are sufficient to generate left/right asymmetry in cultured embryos (Shinohara et al., 2012), this observation does not preclude the possibility that the node organization is abnormal in *Pofut2* epiblast mutants.

3.6. Loss of ADAMTS9 function is likely responsible for gastrulation defects in Pofut2 mutants

Since elimination of *Adamts9* was reported to result in early embryonic lethality in mice (Dubail and Apte, 2015; Enomoto et al., 2010), and ADAMTS9 contains 15 TSRs, of which 12 contain the required consensus sequence and 9 are known to be *O*-fucosylated by POFUT2 (RSH personal communication), we predicted that loss of ADAMTS9 function in *Pofut2* mutants might be responsible for the defects in gastrulation. To test this hypothesis, we evaluated the effects of the *Adamts9* knockout using gross morphology of whole embryos, hematoxylin and eosin staining of sectioned embryos, and *in situ* hybridization to examine markers of extraembryonic ectoderm and mesoderm differentiation (Fig. 4 and Supplementary Fig. 4). E 6.5 wild-type and *Adamts9* mutant embryos were morphologically indistinguishable, suggesting a normal arrangement of extraembryonic and embryonic tissues (not shown). However, by E 7.5 the *Adamts9* mutants were clearly distinguishable from their wild-type littermates. At E 7.5, wild-type littermates had undergone gastrulation, and the amnion and chorion were formed (Fig. 4A–B′). Like *Pofut2* mutants, the tissues in E 7.5 *Adamts9* mutants were disorganized, and mesoderm was lacking (Fig. 4C–D′). Occasionally, the epiblast was completely separated from the extraembryonic ectoderm by the parietal endoderm layer and the visceral endoderm was highly folded (Supplementary

Fig. 4). Consistent with the absence of visible mesoderm, the *Adamts9* mutants failed to maintain expression of *Bmp4*, expressed *Snail1* at most weakly, and activated *T* in only 1 of 5 mutants. The *Adamts9* mutants also displayed the proximal constriction and abnormal visceral endoderm lacking apical vacuoles. The striking similarity between the *Adamts9* and *Pofut2* knockouts suggested that the gastrulation defects present in the *Pofut2* knockout result from disruption of ADAMTS9 function.

To identify tissues responsible for the gastrulation defects observed in *Adamts9* and *Pofut2* knockouts, we examined the expression of *Adamts9* between E 5.5 and E 7.5 of gestation using whole mount *in situ* hybridization and analysis of β-galactosidase activity in embryos heterozygous for the *Adamts9-lacZ* allele (Fig. 5). *Adamts9* expression was first detected at E 5.5 in the trophoblast giant cells by β-galactosidase activity using the *Adamts9-LacZ* allele (not shown). Between E 6.5 and 7.5, *Adamts9* was expressed in extraembryonic tissues including the trophoblast giant cells and parietal endoderm, and in the embryo derived mesoderm of the extraembryonic allantois, amnion, and chorion (Fig. 5A–G′). These results are consistent with previous analysis of *Adamts9* expression in sectioned embryos (Jungers et al., 2005). In addition, we detected *Adamts9* transcripts in the visceral endoderm adjacent to the ectoplacental cone, in the region where the visceral endoderm transitions to parietal endoderm (Fig. 5A, and C white arrow, and Supplementary Fig. 5); however, we did not detect LacZ activity in this region (Fig. 5F).

In the embryo proper, *Adamts9* was transiently expressed in the anterior primitive streak between E 6.5 and E 7.5 (Fig. 5B–G). Expression of *Adamts9* in the anterior primitive streak peaked by the mid-late primitive streak stage (Fig. 5C) and subsequently declined (Fig. 5D–E). We also detected β-galactosidase (β-gal) positive cells between the epiblast and surface endoderm and intercalated into the surface layer, suggesting that cells expressing *Adamts9* were fated to become definitive endoderm and/or axial mesoderm (Fig. 5F–G′). Since *Adamts9* transcripts were only localized to the anterior primitive streak, the β-gal staining in the anterior mesendoderm layer (Fig. 5F–G′) likely results from persistent β-gal activity in cells that originated from the anterior primitive streak.

3.7. Extraembryonic ADAMTS9 is essential for mouse gastrulation

Given the similarity between the *Pofut2* and *Adamts9* knockouts, and the requirement for POFUT2 in the extraembryonic tissues for normal gastrulation (Fig. 2), we hypothesized that loss of ADAMTS9 function in either the trophoblast giant cells, parietal endoderm, or proximal visceral endoderm was responsible for the gastrulation defects present in the *Pofut2* knockout. To test this hypothesis, we examined the effects of Sox2::Cre mediated deletion of *Adamts9* in the epiblast on gastrulation (hereafter referred to as *Adamts9* epiblast mutant) (Fig. 5). By E 9.5, wild-type embryos had turned, neural folds had fused, and the heart and somites were visible (Fig. 5H). In comparison, *Adamts9* epiblast mutants were delayed (Fig. 5I–K), had not turned, and had significantly shorter axis. Two of the four *Adamts9* epiblast mutants (Fig. 5J and K) bore striking resemblance to the *Pofut2* epiblast mutants. The significant development of the *Adamts9* epiblast mutants compared to the *Adamts9-del* mutants, provided strong evidence that ADAMTS9 function in the extraembryonic tissues is essential for gastrulation.

3.8. Loss of Pofut2 impairs secretion of ADAMTS9 in HEK293T cells

In cell culture, depletion of POFUT2 using siRNA impairs trafficking and secretion of all tested POFUT2-targets (Niwa et al., 2015; Ricketts et al., 2007; Vasudevan et al., 2015; Wang et al., 2007), the majority of which normally associate with ECM (Tucker, 2004). These results suggest that impaired secretion of ADAMTS9 contributes to defects in *Pofut2* mutants. To test this hypothesis, we analyzed the effects of CRISPR/Cas9 induced *POFUT2* mutations in HEK293T cells on secretion of transfected myc-tagged ADAMTS9 in cell culture (Fig. 6A), since specific ADAMTS9 antibodies are not available to directly test the localization/secretion of ADAMTS9 in mouse *Pofut2* mutants. ADAMTS9 was secreted from control HEK293T cells with intact *POFUT2* (Fig. 6A, left). Although ADAMTS9 was present in the cell lysate of *POFUT2* null HEK293T cells, ADAMTS9 was not secreted into the medium unless co-transfected with *POFUT2* (Fig. 6A, right). These results demonstrated that *O*-fucosylation of ADAMTS9 TSRs by POFUT2 was essential for secretion of ADAMTS9, and together with the phenotype of *Adamts9* mutant embryos suggested that *O*-fucosylated ADAMTS9 modulation of the extraembryonic ECM properties or cell/matrix interactions is essential for mouse gastrulation.

4. Discussion

In this study, we demonstrated that *O*-fucosylation of POFUT2 target proteins was essential for maintaining the organization of epithelia needed for progression of mouse gastrulation. We propose that differences between the *Pofut2* mutant phenotype observed in this study compared to the previously published report likely result from genetic background differences. The similarity between the *Pofut2* and *Adamts9* mutant phenotypes and defective secretion of ADAMTS9 in *Pofut2* mutant cells suggest that loss of ADAMTS9 function was likely responsible for the gastrulation defects in *Pofut2* mutants. Combined, the pattern of *Adamts9* expression and developmental abnormalities in the *Pofut2* and *Adamts9* epiblast mutants provided evidence that loss of ADAMTS9 function in one or more of the extraembryonic cell types (trophectoderm, parietal endoderm, or visceral endoderm adjacent to the ectoplacental cone) was responsible for blocking gastrulation in *Pofut2* and *Adamts9* mutants (Fig. 6B). Moreover, the abnormalities present in the *Pofut2* epiblast mutants suggested that *O*-fucosylation of POFUT2 targets was also essential for axis elongation. Since the early anterior primitive streak domain of *Adamts9* expression correlates with cells fated to become the definitive endoderm (Lawson et al., 1986; Lawson and Pedersen, 1987; Tam and Beddington, 1987, 1992) and the epithelial node (Poelmann, 1981; Sulik et al., 1994; Yamanaka et al., 2007), and *Adamts9* epiblast mutants also displayed truncated axis, loss of ADAMTS9 function in these cell types could contribute to the axial defects observed in *Pofut2* epiblast mutants (Fig. 2). However, given the differences in the severity of the axis elongation defects in *Adamts9* epiblast mutants, it is possible that other POFUT2 targets may help to compensate for loss of ADAMTS9 function by epiblast cells, or that there is some residual ADAMTS9 activity after loss of POFUT2.

Defective secretion of ADAMTS9 in *POFUT2*-null HEK293T cells suggested that abnormalities observed in *Pofut2* mutants could result from altered properties of the ECM. ADAMTS9 is known to process aggrecan and/or versican (Somerville et al., 2003), and

depletion of ADAMTS9 during development of the heart, palate, umbilical cord, and regression of interdigital web leads to accumulation of versican and abnormalities in the ECM (Dubail et al., 2014; McCulloch et al., 2009; Enomoto et al., 2010; Kern et al., 2010). Neither aggrecan nor versican are known to be expressed in the gastrulating embryo. Therefore, we do not fully understand how loss of *Pofut2* or *Adamts9* leads to the defects in gastrulation and axial elongation, and it could be *via* proteolysis of as yet unidentified substrates. However, since an *Adamts9* mutant that generates a membrane bound form of ADAMTS9 (*Adamts9*-Gt) develops considerably further than the *Adamts9* or *Pofut2* null embryos (Nandadasa et al., 2015), we hypothesize that the matrix of the early gastrula requires the local rather than long range action of ADAMTS9. This effect could occur through ADAMTS metalloproteinase activity or alternatively could occur through direct interaction with other cells thru ADAMTS9's CSVTCG motif (thought to mediate binding to the cell surface molecule CD36 (Asch et al., 1992)) or through ADAMTS9's BBXB motif (thought to mediate interactions with heparin and sulfatide in the matrix (Proudfoot et al., 2001)).

Clues to understanding how loss of ADAMTS9 alters the properties of the ECM come from analysis of the *Caenorhabditis elegans gon-1* mutants (Blelloch et al., 1999) where the ECM is comprised of a simpler basement membrane composed of primarily of laminin, type IV collagen, nidogen, and perlecan (Kim and Nishiwaki, 2015). In *C. elegans*, the *Adamts9* homologue, *gon-1,* is essential for migration of the gonadal distal tip cell (Blelloch et al., 1999). Genetic interaction studies demonstrated that *gon-1* and *Fibulin* (*fbl*-1) (encodes a minor component of the basement membrane) function antagonistically in regulating distal tip cell migration, and that a dominant mutation in type IV collagen α1 chain (*emb*-9 *(tk75)*) relieves distal tip migration defects observed in *fbl-1* mutants and exacerbates the effects of *gon-1* mutants (Hesselson et al., 2004; Kubota et al., 2012). These results suggest that GON-1 and FBL-1 mediated alteration of collagen IV organization directs the migration of the distal tip cells. It is intriguing to speculate that similar alterations in collagen IV organization could contribute to the gastrulation defects observed in *Pofut2/Adamts9* mutants, since basement membranes are the primary ECM assemblies at the pregastrulation stage. However, since collagen IV is not a known substrate for ADAMTS9 or GON-1 (Somerville et al., 2004), changes in collagen IV organization are likely modulated by an as yet unidentified ADAMTS9/GON-1 target or through an as yet unidentified non-proteolytic function of ADAMTS9/GON-1.

The ability of teratomas produced from *Pofut2-RST434* mutant epiblast to differentiate into a variety of mesoderm derived tissues provides evidence that the inability of *Pofut2* mutant cells to differentiate results from a lack of signal rather than the inability to respond to signal (Du et al., 2010). For this reason, we predict that a major factor inhibiting mesoderm induction in *Pofut2* or *Adamts9* mutants is the altered characteristics of the extraembryonic ectoderm and in the most extreme cases a displacement of extraembryonic ectoderm (Supplementary Fig. 4; Fig. 6B). A similar block in mesoderm differentiation is observed when the extraembryonic ectoderm is physically removed from epiblast explants (Beck et al., 2002; Rodriguez et al., 2005). Altered characteristics of the extraembryonic ectoderm could also explain the lack of mesoderm in *Pofut2* mutants, since the extraembryonic ectoderm is a source of proprotein convertases that are essential to maintain *Nodal*

expression in the epiblast (Ben-Haim et al., 2006), and expression of *Bmp4* in the extraembryonic ectoderm induces *Wnt3* in the epiblast, which amplifies expression of epiblast *Nodal*; together Wnt and Nodal signaling mediate mesoderm induction (Ben-Haim et al., 2006). Altered characteristics of the extraembryonic ectoderm could also be responsible for changes in the characteristics of the *Pofut2/Adamts9* mutant visceral endoderm, since BMP signals are important for maintaining visceral endoderm characteristics in extraembryonic endoderm stem cell cultures (Paca et al., 2012).

It is intriguing to speculate that ADAMTS9 function in the visceral endoderm functions locally to anchor the most proximal visceral cells to the ECM or ectoplacental cone cells at the region of transition between the visceral and parietal endoderm (Fig. 6B). In this model, impaired secretion of ADAMTS9 in *Pofut2* mutants or loss of *Adamts9* leads to slippage of the parietal/visceral endoderm layers, resulting in mechanical displacement or altered characteristics of the extraembryonic ectoderm and compression of the epiblast (Fig. 6B). This model is consistent with the ability of the wild-type extraembryonic tissues to rescue the gastrulation defects in *Pofut2* and *Adamts9* epiblast mutants (Fig. 2). Altered properties of Reichert's membrane could also contribute to the observed densely packed parietal endoderm, the ruffled/folded characteristics of the visceral endoderm in *Pofut2* and *Adamts9* mutants (Figs. 1 and 4), and increased laminin staining observed in Reichert's membrane of *Pofut2* mutants (Du et al., 2010).

Analogous slippage of embryonic tissues was observed in *C. elegans* mutants lacking hemicentin, a component of the hemidesmosome in the developing gonad (Morrissey et al., 2014). Mouse Hemicentin-1 is also a predicted target of POFUT2 (Du et al., 2010). Since hemicentins are important for maintaining the architectural integrity of vertebrate tissues and organs (reviewed in Xu et al. (2013)), disruption of cell-ECM connections could also contribute to disorganization of epithelia in the *Pofut2* mutants. However, since the mouse *Hemicentin-1* knockout disrupts early cleavage divisions and results in pre-implantation lethality, loss of *Pofut2* must not completely block Hemicentin-1 function (Xu and Vogel, 2011).

The *Pofut2* and *Adamts9* conditional epiblast mutants presented a new set of phenotypes not observed in the *Pofut2* or *Adamts9* knockout, providing evidence for the role of POFUT2 target proteins in axis elongation and morphogenesis of the amnion. In mouse, axis elongation problems have been reported when mutations disrupt node and notochord formation (*Hnf3β* and *Lulu*) (Dufort et al., 1998; Lee and Anderson, 2008; Lee et al., 2010), interfere with cell polarity (for example *Vangl2/Lp* and *Chuhzoi*) (Kibar et al., 2001; Paudyal et al., 2010; Wilson and Wyatt, 1992), or disrupt amnion morphogenesis (*Bmp2, Foxf1, Pagr1a*, and *Fn1*) (George et al., 1993; Kumar et al., 2014; Mahlapuu et al., 2001; Zhang and Bradley, 1996). Compared to any of these mutants, the severely truncated axis in *Pofut2* epiblast mutants suggest that multiple factors likely contribute to the observed axis elongation defects. The persistent attachment of the developing chorion and the amnion observed in *Pofut2* epiblast mutants is similar to that observed in *Fn1* mutants (George et al., 1993). For this reason, we predict that loss of *Adamts9* or *Pofut2* contributes in part to the axis elongation defects by altering the properties of the amnion/chorion membrane ECM

similar to a *Fn1* mutants (George et al., 1993). This is consistent with the expression of *Adamts9* in the extraembryonic mesoderm.

Since activation of *Lefty2* in the lateral plate mesoderm depends upon functioning node cilia, and *Lefty2* is activated in *Pofut2* epiblast mutants (Fig. 4), defects in early node morphogenesis likely do not contribute to the axis elongation defects. However, because of the wide distribution of *T* and *Foxa2* transcripts in the trunk notochord precursors at the early headfold stage, loss of POFUT2 could interfere with later node function. Moreover, the broad distribution of *T* and *Foxa2* raise the possibility that loss of *Pofut2* in the epiblast derived cells alter the properties of the underlying ECM that disrupt convergent extension movements or alter the properties of the definitive endoderm. In the future, we will use the conditional deletion strategy to distinguish whether axial elongation defects result from defects in the amnion, epiblast or epiblast-derived definitive endoderm and notochord. The *Pofut2* and *Adamts9* conditional mutants will also provide valuable tools to identify changes in the extracellular matrix and evaluate the consequence of these changes on morphogenesis.

Supplementary Material

Refer to Web version on PubMed Central for supplementary material.

Acknowledgments

Funding

This work was supported by the National Institutes of Health Grants: CA123071 to RSH and BH, and HL107147 to SSA, and funding from the Georgia Research Alliance to RSH.

We thank Drs. David Matus, Howard Sirotkin, and Gerald Thomsen for critical evaluation of the manuscript, Joel Israel at Mc Clain Laboratories, Smithtown, NY for assistance with *Pofut2* embryo sectioning and staining, and Julie Nelson at CTEGD Cytometry Shared Resource Laboratory at University of Georgia for technical assistance.

References

Adams JC, Tucker RP. The thrombospondin type 1 repeat (TSR) superfamily: diverse proteins with related roles in neuronal development. Dev Dyn. 2000; 218:280–299. [PubMed: 10842357]

Apte SS. A disintegrin-like and metalloprotease (reprolysin-type) with thrombospondin type 1 motif (ADAMTS) superfamily: functions and mechanisms. J Biol Chem. 2009; 284:31493–31497. [PubMed: 19734141]

Asch AS, Silbiger S, Heimer E, Nachman RL. Thrombospondin sequence motif (CSVTCG) is responsible for CD36 binding. Biochem Biophys Res Commun. 1992; 182:1208–1217. [PubMed: 1371676]

Basu B, Brueckner M. Cilia multifunctional organelles at the center of vertebrate left-right asymmetry. Curr Top Dev Biol. 2008; 85:151–174. [PubMed: 19147005]

Beck S, Le Good JA, Guzman M, Ben Haim N, Roy K, Beermann F, Constam DB. Extraembryonic proteases regulate Nodal signalling during gastrulation. Nat Cell Biol. 2002; 4:981–985. [PubMed: 12447384]

Ben-Haim N, Lu C, Guzman-Ayala M, Pescatore L, Mesnard D, Bischofberger M, Naef F, Robertson EJ, Constam DB. The nodal precursor acting via activin receptors induces mesoderm by maintaining a source of its convertases and BMP4. Dev Cell. 2006; 11:313–323. [PubMed: 16950123]

Blelloch R, Anna-Arriola SS, Gao D, Li Y, Hodgkin J, Kimble J. The gon-1 gene is required for gonadal morphogenesis in *Caenorhabditis elegans*. Dev Biol. 1999; 216:382–393. [PubMed: 10588887]

Chen CI, Keusch JJ, Klein D, Hess D, Hofsteenge J, Gut H. Structure of human POFUT2: insights into thrombospondin type 1 repeat fold and O-fucosylation. EMBO J. 2012; 31:3183–3197. [PubMed: 22588082]

Downs KM, Davies T. Staging of gastrulating mouse embryos by morphological landmarks in the dissecting microscope. Development. 1993; 118:1255–1266. [PubMed: 8269852]

Du J, Takeuchi H, Leonhard-Melief C, Shroyer KR, Dlugosz M, Haltiwanger RS, Holdener BC. O-Fucosylation of thrombospondin type 1 repeats restricts epithelial to mesenchymal transition (EMT) and maintains epiblast plur-ipotency during mouse gastrulation. Dev Biol. 2010; 346:25–38. [PubMed: 20637190]

Dubail J, Apte SS. Insights on ADAMTS proteases and ADAMTS-like proteins from mammalian genetics. Matrix Biol. 2015; 44–46:24–37. http://dx.doi.org/10.1016/j.matbio.2015.03.001.

Dubail J, Aramaki-Hattori N, Bader HL, Nelson CM, Katebi CM, Matuska B, Olsen BR, Apte SS. A new Adamts9 conditional mouse allele identifies its non-redundant role in interdigital web regression. Genesis. 2014; 52(7):702–712. http://dx.doi.org/10.1002/dvg.22784. [PubMed: 24753090]

Dufort D, Schwartz L, Harpal K, Rossant J. The transcription factor HNF3beta is required in visceral endoderm for normal primitive streak morphogenesis. Development. 1998; 125:3015–3025. [PubMed: 9671576]

Enomoto H, Nelson CM, Somerville RP, Mielke K, Dixon LJ, Powell K, Apte SS. Cooperation of two ADAMTS metalloproteases in closure of the mouse palate identifies a requirement for versican proteolysis in regulating palatal mesenchyme proliferation. Development. 2010; 137:4029–4038. [PubMed: 21041365]

George EL, Georges-Labouesse EN, Patel-King RS, Rayburn H, Hynes RO. Defects in mesoderm, neural tube and vascular development in mouse embryos lacking fibronectin. Development. 1993; 119:1079–1091. [PubMed: 8306876]

Hesselson D, Newman C, Kim KW, Kimble J. GON-1 and flbulin have antagonistic roles in control of organ shape. Curr Biol. 2004; 14:2005–2010. [PubMed: 15556862]

Hsieh JC, Lee L, Zhang L, Wefer S, Brown K, DeRossi C, Wines ME, Rosenquist T, Holdener BC. Mesd encodes an LRP5/6 chaperone essential for specification of mouse embryonic polarity. Cell. 2003; 112:355–367. [PubMed: 12581525]

Hubmacher D, Apte SS. Genetic and functional linkage between ADAMTS superfamily proteins and fibrillin-1: a novel mechanism influencing microfibril assembly and function. Cell Mol Life Sci. 2011; 68:3137–3148. [PubMed: 21858451]

Jungers KA, Le Goff C, Somerville RP, Apte SS. Adamts9 is widely expressed during mouse embryo development. Gene Expr Patterns. 2005; 5:609–617. [PubMed: 15939373]

Kern CB, Wessels A, McGarity J, Dixon LJ, Alston E, Argraves WS, Geeting D, Nelson CM, Menick DR, Apte SS. Reduced versican cleavage due to Adamts9 haploinsufficiency is associated with cardiac and aortic anomalies. Matrix Biol. 2010; 29:304–316. [PubMed: 20096780]

Kibar Z, Vogan KJ, Groulx N, Justice MJ, Underhill DA, Gros P. Ltap, a mammalian homolog of Drosophila Strabismus/Van Gogh, is altered in the mouse neural tube mutant Loop-tail. Nat Genet. 2001; 28:251–255. [PubMed: 11431695]

Kim HS, Nishiwaki K. Control of the basement membrane and cell migration by ADAMTS proteinases: lessons from *C. elegans* genetics. Matrix Biol. 2015; 44–46:64–69.

Kinder SJ, Tsang TE, Wakamiya M, Sasaki H, Behringer RR, Nagy A, Tam PP. The organizer of the mouse gastrula is composed of a dynamic population of progenitor cells for the axial mesoderm. Development. 2001; 128:3623–3634. [PubMed: 11566865]

Koo BH, Coe DM, Dixon LJ, Somerville RP, Nelson CM, Wang LW, Young ME, Lindner DJ, Apte SS. ADAMTS9 is a cell-autonomously acting, anti-angiogenic metalloprotease expressed by microvascular endothelial cells. Am J Pathol. 2010; 176:1494–1504. [PubMed: 20093484]

Kozma K, Keusch JJ, Hegemann B, Luther KB, Klein D, Hess D, Haltiwanger RS, Hofsteenge J. Identification and characterization of a beta1,3-glucosyltransferase that synthesizes the Glc-

beta1,3-Fuc disaccharide on thrombospondin type 1 repeats. J Biol Chem. 2006; 281:36742–36751. [PubMed: 17032646]

Kubota Y, Nagata K, Sugimoto A, Nishiwaki K. Tissue architecture in the Caenorhabditis elegans gonad depends on interactions among fibulin-1, type IV collagen and the ADAMTS extracellular protease. Genetics. 2012; 190:1379–1388. [PubMed: 22298704]

Kumar A, Lualdi M, Loncarek J, Cho YW, Lee JE, Ge K, Kuehn MR. Loss of function of mouse Pax-Interacting Protein 1-associated glutamate rich protein 1a (Pagr1a) leads to reduced Bmp2 expression and defects in chorion and amnion development. Dev Dyn. 2014; 243:937–947. [PubMed: 24633704]

Kwon GS, Viotti M, Hadjantonakis AK. The endoderm of the mouse embryo arises by dynamic widespread intercalation of embryonic and extraembryonic lineages. Dev Cell. 2008; 15:509–520. [PubMed: 18854136]

Lawson KA, Pedersen RA. Cell fate, morphogenetic movement and population kinetics of embryonic endoderm at the time of germ layer formation in the mouse. Development. 1987; 101:627–652. [PubMed: 3502998]

Lawson KA, Meneses JJ, Pedersen RA. Cell fate and cell lineage in the endoderm of the presomite mouse embryo, studied with an intracellular tracer. Dev Biol. 1986; 115:325–339. [PubMed: 3709966]

Lee JD, Anderson KV. Morphogenesis of the node and notochord: the cellular basis for the establishment and maintenance of left-right asymmetry in the mouse. Dev Dyn. 2008; 237:3464–3476. [PubMed: 18629866]

Lee JD, Migeotte I, Anderson KV. Left-right patterning in the mouse requires Epb4.1l5-dependent morphogenesis of the node and midline. Dev Biol. 2010; 346:237–246. [PubMed: 20678497]

Lesnik Oberstein SA, Kriek M, White SJ, Kalf ME, Szuhai K, den Dunnen JT, Breuning MH, Hennekam RC. Peters Plus syndrome is caused by mutations in B3GALTL, a putative glycosyltransferase. Am J Hum Genet. 2006; 79:562–566. [PubMed: 16909395]

Luo Y, Koles K, Vorndam W, Haltiwanger RS, Panin VM. Protein O-fucosyltransferase 2 adds O-fucose to thrombospondin type 1 repeats. J Biol Chem. 2006; 281:9393–9399. [PubMed: 16464857]

Mahlapuu M, Ormestad M, Enerback S, Carlsson P. The forkhead transcription factor Foxf1 is required for differentiation of extra-embryonic and lateral plate mesoderm. Development. 2001; 128:155–166. [PubMed: 11124112]

McCulloch DR, Nelson CM, Dixon LJ, Silver DL, Wylie JD, Lindner V, Sasaki T, Cooley MA, Argraves WS, Apte SS. ADAMTS metalloproteases generate active versican fragments that regulate interdigital web regression. Dev Cell. 2009; 17:687–698. [PubMed: 19922873]

Montcouquiol M, Rachel RA, Lanford PJ, Copeland NG, Jenkins NA, Kelley MW. Identification of Vangl2 and Scrb1 as planar polarity genes in mammals. Nature. 2003; 423:173–177. [PubMed: 12724779]

Morrissey MA, Keeley DP, Hagedorn EJ, McClatchey ST, Chi Q, Hall DH, Sherwood DR. B-LINK: a hemicentin, plakin, and integrin-dependent adhesion system that links tissues by connecting adjacent basement membranes. Dev Cell. 2014; 31:319–331. [PubMed: 25443298]

Nandadasa S, Nelson CM, Apte SS. ADAMTS9-mediated extracellular matrix dynamics regulates umbilical cord vascular smooth muscle differentiation and rotation. Cell Rep. 2015

Niwa Y, Suzuki T, Dohmae N, Simizu S. O-fucosylation of CCN1 is required for its secretion. FEBS Lett. 2015; 589:3287–3293. [PubMed: 26424659]

Paca A, Seguin CA, Clements M, Ryczko M, Rossant J, Rodriguez TA, Kunath T. BMP signaling induces visceral endoderm differentiation of XEN cells and parietal endoderm. Dev Biol. 2012; 361:90–102. [PubMed: 22027433]

Paudyal A, Damrau C, Patterson VL, Ermakov A, Formstone C, Lalanne Z, Wells S, Lu X, Norris DP, Dean CH, Henderson DJ, Murdoch JN. The novel mouse mutant, chuzhoi, has disruption of Ptk7 protein and exhibits defects in neural tube, heart and lung development and abnormal planar cell polarity in the ear. BMC Dev Biol. 2010; 10:87. [PubMed: 20704721]

Poelmann RE. The head-process and the formation of the definitive endoderm in the mouse embryo. Anat Embryol. 1981; 162:41–49. [PubMed: 7283172]

Proudfoot AE, Fritchley S, Borlat F, Shaw JP, Vilbois F, Zwahlen C, Trkola A, Marchant D, Clapham PR, Wells TN. The BBXB motif of RANTES is the principal site for heparin binding and controls receptor selectivity. J Biol Chem. 2001; 276:10620–10626. [PubMed: 11116158]

Ricketts LM, Dlugosz M, Luther KB, Haltiwanger RS, Majerus EM. O-fucosylation is required for ADAMTS13 secretion. J Biol Chem. 2007; 282:17014–17023. [PubMed: 17395589]

Rodriguez TA, Srinivas S, Clements MP, Smith JC, Beddington RS. Induction and migration of the anterior visceral endoderm is regulated by the extra-embryonic ectoderm. Development. 2005; 132:2513–2520. [PubMed: 15857911]

Sato T, Sato M, Kiyohara K, Sogabe M, Shikanai T, Kikuchi N, Togayachi A, Ishida H, Ito H, Kameyama A, Gotoh M, Narimatsu H. Molecular cloning and characterization of a novel human beta1,3-glucosyltransferase, which is localized at the endoplasmic reticulum and glucosylates O-linked fucosylglycan on thrombospondin type 1 repeat domain. Glycobiology. 2006; 16:1194–1206. [PubMed: 16899492]

Shinohara K, Kawasumi A, Takamatsu A, Yoshiba S, Botilde Y, Motoyama N, Reith W, Durand B, Shiratori H, Hamada H. Two rotating cilia in the node cavity are sufficient to break left-right symmetry in the mouse embryo. Nat Commun. 2012; 3:622. [PubMed: 22233632]

Shiratori H, Hamada H. The left-right axis in the mouse: from origin to morphology. Development. 2006; 133:2095–2104. [PubMed: 16672339]

Shumacher A, Faust C, Magnuson T. Positional cloning of a global regulator of anterior-posterior patterning in mice. Nature. 1996; 383:250–253. [PubMed: 8805699]

Somerville RP, Jungers KA, Apte SS. Discovery and characterization of a novel, widely expressed metalloprotease, ADAMTS10, and its proteolytic activation. J Biol Chem. 2004; 279:51208–51217. [PubMed: 15355968]

Somerville RP, Longpre JM, Jungers KA, Engle JM, Ross M, Evanko S, Wight TN, Leduc R, Apte SS. Characterization of ADAMTS-9 and ADAMTS-20 as a distinct ADAMTS subfamily related to *Caenorhabditis elegans* GON-1. J Biol Chem. 2003; 278:9503–9513. [PubMed: 12514189]

Sulik K, Dehart DB, Iangaki T, Carson JL, Vrablic T, Gesteland K, Schoenwolf GC. Morphogenesis of the murine node and notochordal plate. Dev Dyn. 1994; 201:260–278. [PubMed: 7881129]

Taibi AV, Lighthouse JK, Grady RC, Shroyer KR, Holdener BC. Development of a conditional Mesd (mesoderm development) allele for functional analysis of the low-density lipoprotein receptor-related family in defined tissues. PLoS One. 2013; 8:e75782. [PubMed: 24124512]

Tam PP, Beddington RS. The formation of mesodermal tissues in the mouse embryo during gastrulation and early organogenesis. Development. 1987; 99:109–126. [PubMed: 3652985]

Tam PP, Beddington RS. Establishment and organization of germ layers in the gastrulating mouse embryo. Ciba Found Symp. 1992; 165:27–41. Discussion 42-29. [PubMed: 1516473]

Thomas M, Lu JJ, Ge Q, Zhang C, Chen J, Klibanov AM. Full deacylation of polyethylenimine dramatically boosts its gene delivery efficiency and specificity to mouse lung. Proc Natl Acad Sci USA. 2005; 102:5679–5684. [PubMed: 15824322]

Tucker RP. The thrombospondin type 1 repeat superfamily. Int J Biochem Cell Biol. 2004; 36:969–974. [PubMed: 15094110]

Valero-Gonzalez J, Leonhard-Melief C, Lira-Navarrete E, Jimenez-Oses G, Hernandez-Ruiz C, Pallares MC, Yruela I, Vasudevan D, Lostao A, Corzana F, Takeuchi H, Haltiwanger RS, Hurtado-Guerrero R. A proactive role of water molecules in acceptor recognition by protein O-fucosyltransferase 2. Nat Chem Biol. 2016; 12:240–246. [PubMed: 26854667]

Vasudevan D, Takeuchi H, Johar SS, Majerus E, Haltiwanger RS. Peters plus syndrome mutations disrupt a noncanonical ER quality-control mechanism. Curr Biol. 2015; 25:286–295. [PubMed: 25544610]

Wang LW, Dlugosz M, Somerville RP, Raed M, Haltiwanger RS, Apte SS. O-fucosylation of thrombospondin type 1 repeats in ADAMTS-like-1/punctin-1 regulates secretion: implications for the ADAMTS superfamily. J Biol Chem. 2007; 282:17024–17031. [PubMed: 17395588]

Wang Y, Guo N, Nathans J. The role of Frizzled3 and Frizzled6 in neural tube closure and in the planar polarity of inner-ear sensory hair cells. J Neurosci. 2006; 26:2147–2156. [PubMed: 16495441]

Wilson DB, Wyatt DP. Abnormal elevation of the neural folds in the loop-tail mutant mouse. Acta Anat. 1992; 143:89–95. [PubMed: 1598821]

Xu X, Vogel BE. A secreted protein promotes cleavage furrow maturation during cytokinesis. Curr Biol. 2011; 21:114–119. [PubMed: 21215633]

Xu X, Xu M, Zhou X, Jones OB, Moharomd E, Pan Y, Yan G, Anthony DD, Isaacs WB. Specific structure and unique function define the hemicentin. Cell Biosci. 2013; 3:27. [PubMed: 23803222]

Yamanaka Y, Tamplin OJ, Beckers A, Gossler A, Rossant J. Live imaging and genetic analysis of mouse notochord formation reveals regional morphogenetic mechanisms. Dev Cell. 2007; 13:884–896. [PubMed: 18061569]

Zhang H, Bradley A. Mice deficient for BMP2 are nonviable and have defects in amnion/chorion and cardiac development. Development. 1996; 122:2977–2986. [PubMed: 8898212]

Appendix A. Supplementary material

Supplementary data associated with this article can be found in the online version at http://dx.doi.org/10.1016/j.ydbio.2016.05.038.

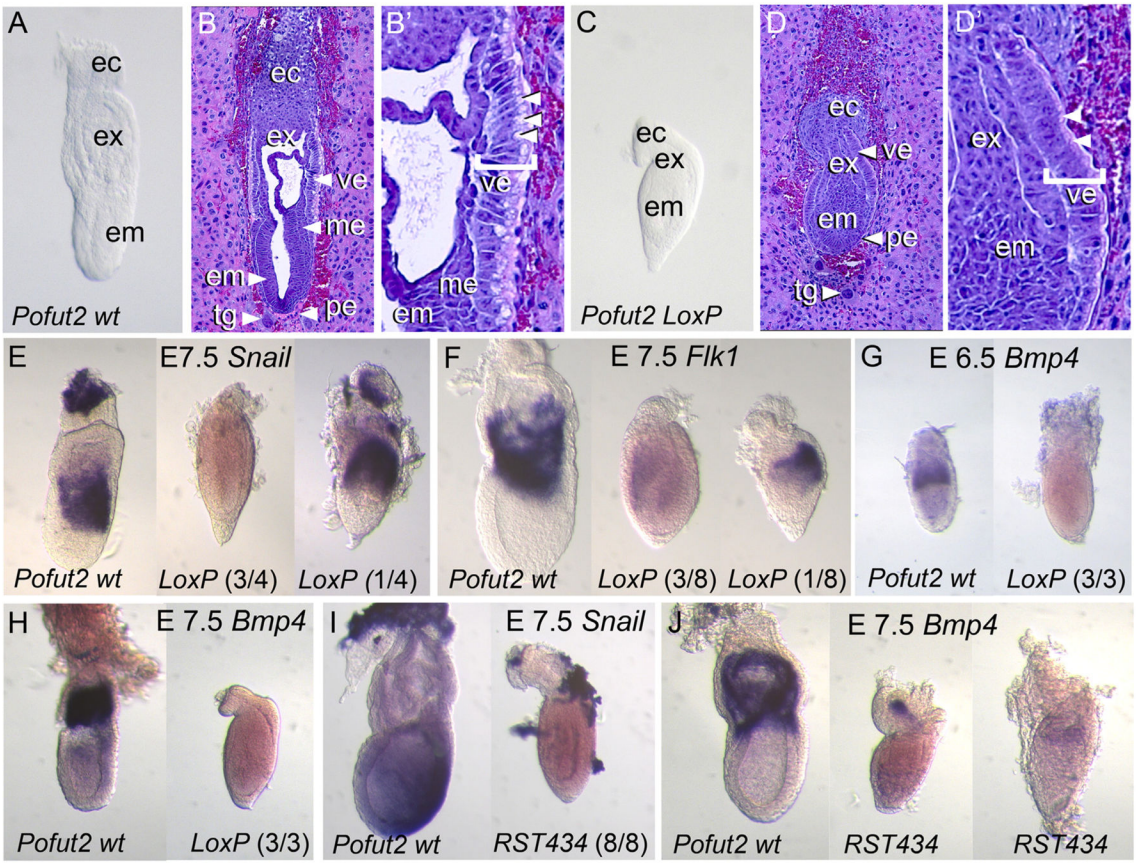

Fig. 1.

POFUT2 is essential for maintaining epithelial organization and mesoderm differentiation. (A–D′) Comparison of E 7.5 *Pofut2* wild-type (*Pofut2 wt*) and *Pofut2* knockout embryos (*Pofut2-LoxP*) by gross morphology (A and C) and hematoxylin and eosin staining of sections (B and D). Embryo orientation: proximal up and distal down; anterior left and posterior right. (A–B′) wild-type embryos have well-defined embryonic (embryonic ectoderm, ec; mesoderm, me) and extraembryonic tissues (ectoplacental cone, ec; extraembryonic ectoderm, ex; embryonic ectoderm, em; visceral endoderm, ve; parietal endoderm, pe; trophoblast giant cells, tg). (B′) The proximal visceral endoderm (bracketed) is highly polarized and has large apical vacuoles (arrowheads). (C–D′) In contrast, tissues in *Pofut2* knockout embryos are highly compressed, mesoderm is not clearly visible, and extraembryonic structures derived from mesoderm are absent. (D′) The *Pofut2* knockout visceral endoderm, although polarized, lacks large apical vacuoles (arrowheads). (E–J) Comparison of mesodermal (*Snail* and *Flk1*) and mesodermal and extraembryonic ectoderm (*Bmp4*) marker expression using whole mount *in situ* hybridization. Where the expression patterns varied in *Pofut2* mutants, representative embryos are shown with number of embryos in indicated in parenthesis. (E–F) Comparison of gene expression in wild-type (left) and *Pofut2-LoxP* mutants (right). In contrast to E 7.5 wild-type embryos, the majority of *Pofut2* mutants fail to express these genes, or expressed them at lower levels. Note that 4/8 *Pofut2-LoxP* mutants did not express *Flk1* (not shown). (I, J) Comparison of *Snail* (I) and *Bmp4* (J) expression in wild-type (left) and *Pofut2-RST434* mutant littermates (right).

Pofut2-RST434 mutants lack *Snail* mRNA and show only limited expression of *Bmp4* in the extraembryonic region. In this study, the *Pofut2-RST434* had been back-crossed more than 20 generations to C57BL/6J. Embryos are oriented proximal up and distal down. Wild-type embryos are oriented anterior to the left; Anterior posterior orientation of *Pofut2* mutants is not known.

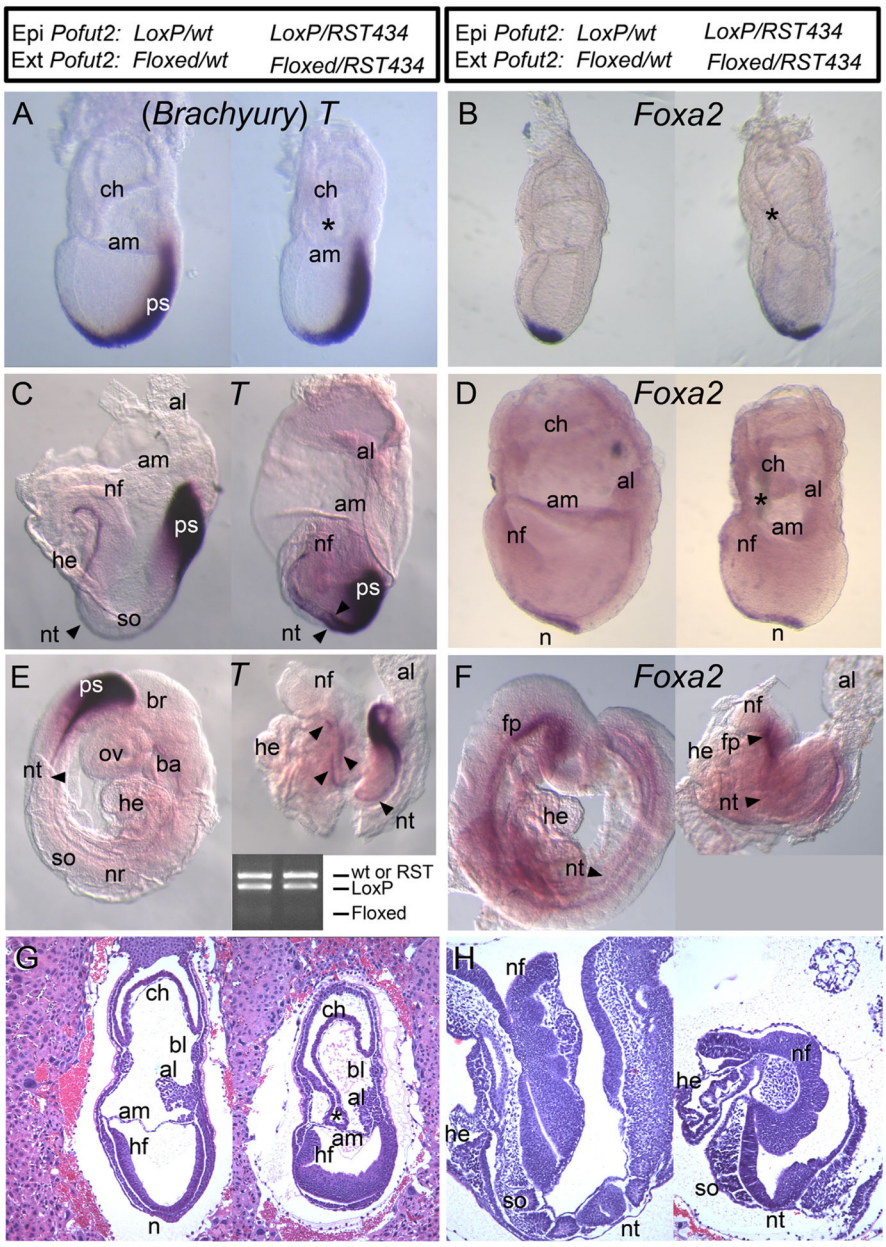

Fig. 2.

Pofut2 activity in the epiblast is essential for axis elongation. The genotypes of the epiblast (Epi) and extraembryonic (Ext) tissues in the embryo pairs (control on the left and epiblast mutants on the right) are indicated at the top of the figure. To evaluate the effects of deleting *Pofut2* in the epiblast using Sox2::Cre, embryos were obtained between E 7.5 (A–B, G) and 8.5 (C–F, H) and were processed for whole-mount *in situ* hybridization expression or were embedded, sectioned, and stained with hematoxylin and eosin to evaluate tissue morphology (G and H). (A, C, and E) *T* was expressed in the primitive streak and notochord of *Pofut2* wild-type and epiblast mutants, suggesting that loss of POFUT2 activity in the extraembryonic tissue was responsible for blocking gastrulation in the *Pofut2* mutants (Fig. 1). Arrowheads in panel E identify discontinuous notochord. (E) Inset shows PCR

genotyping of embryos. Lanes correspond to embryo on the left and right. Full litters for panels C and E are shown in Supplementary Fig. 3 with complete genotyping. (B, D, and F) *Foxa2* was expressed in the anterior primitive streak and emerging mesendoderm at the late primitive streak stage (B), notochord at the early headfold stage (D), and notochord and floorplate at late headfold stage (F) in *Pofut2* wild-type and epiblast mutants. Both *T* and *Foxa2* expression domains were wider and somewhat irregular in shape in the *Pofut2* epiblast mutants compared to wild-type littermates. (G and H) Sagittal sections of *Pofut2* wild-type and epiblast mutant littermates at E 7.5 (G) E 8.5 (H) stained with hematoxylin and eosin. (G) At E 7.5 (late bud stage), the chorion frequently remains attached to the amnion in *Pofut2* epiblast mutants and the epiblast appears disorganized. Persistent attachment of chorion and amnion is indicated by asterisk (*). (H) At E 8.5, there is evidence of heart and somite development in *Pofut2* epiblast mutants. Anterior is to the left, posterior to the right, proximal up, and distal down. Amnion, am; allantois, al; blood islands, bl; brachial arch, ba; brain, br; chorion, ch; heart, he; headfold, hf; neural fold, nf; node, n; notochord, nt; neural tube, nr; optic vesicle, ov; somite, so.

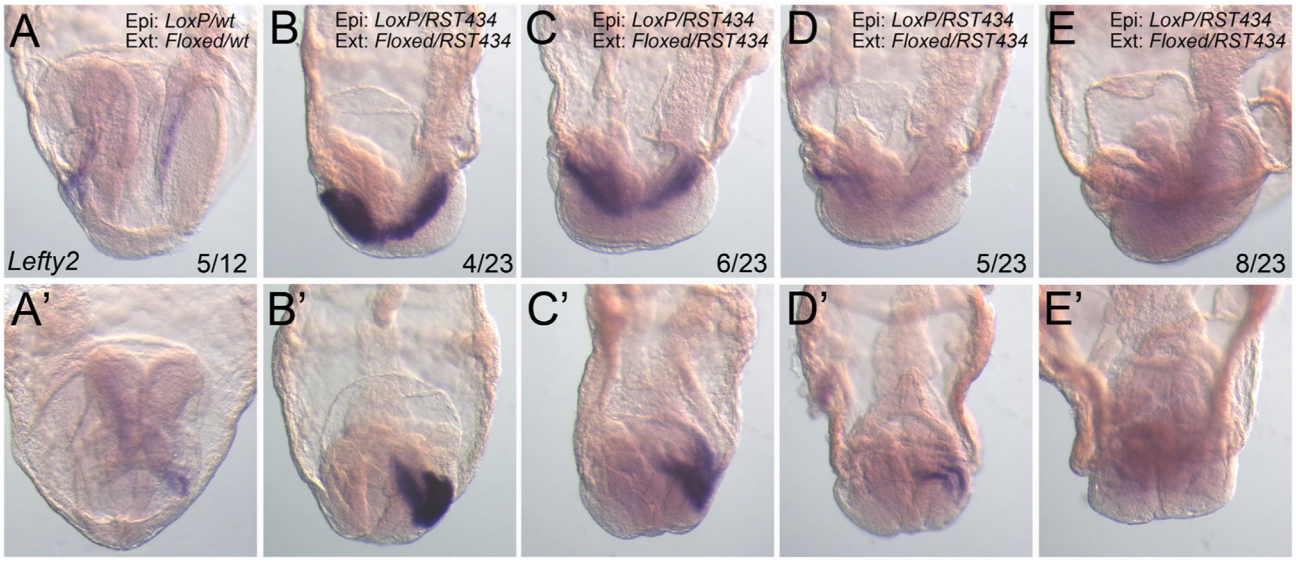

Fig. 3.

Laterality is likely established in *Pofut2* epiblast mutants. Representative whole mount *Lefty2 in situ* hybridization in E8.5 embryos viewed from the left side (anterior to the left) (A–E) or the anterior (A′–E′). The number of *Pofut2* wild-type (*Pofut2 wt)* or *Pofut2* epiblast mutant (*Pofut2 epi mut*) embryos displaying the respective expression pattern is shown as a fraction of total embryos analyzed. (A) In wild-type embryos *Lefty2* was expressed in the lateral plate mesoderm or 5 embryos and extinguished in 7. (B–E) A range of *Lefty2* expression in the lateral plate mesoderm was detected in the majority of *Pofut2* epiblast mutant embryos. Genotype of epiblast (Epi:) and extraembryonic tissues (Ext:) are shown for each embryo.

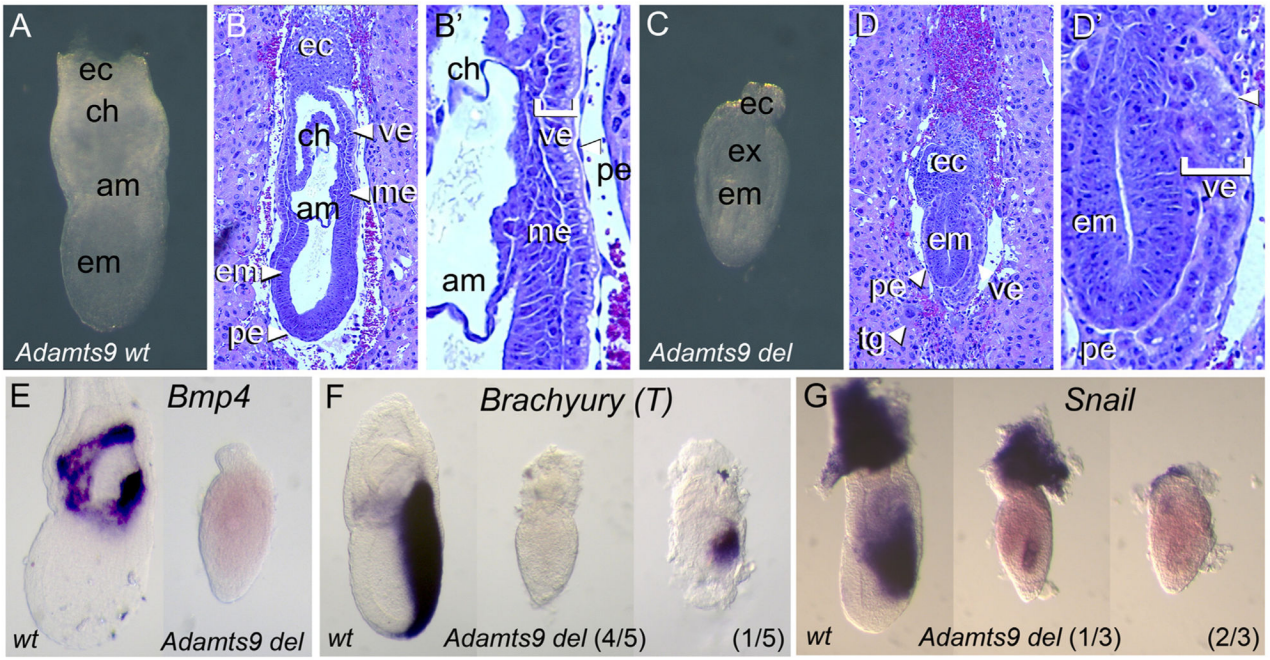

Fig. 4.

Adamts9 null embryos recapitulate the *Pofut2* knockout phenotype. (A–D′) Comparison of gross morphology of E 7.5 *Adamts9* wild-type (*Adamts9 wt*) and *Adamts9* nullembryos (*Adamts9*$^{del/del}$) (A and C) and after hematoxylin and eosin staining of sections (B and D). Wild-type embryos (A and B) are similar to those described in Fig. 1(A–B′). In contrast, the epithelia of *Adamts9* mutants (C–D) were disorganized and the visceral endoderm lacked apical vacuoles, similar to that observed in *Pofut2* knockouts (Fig. 1C–D′). White arrowheads in panel D′ point to the absence of apical vesicles in *Adamts9* mutants. (E–G) Whole-mount *in situ* hybridization comparison of *Adamts9* wild-type and knockout embryos at E 7.5. (E) *Bmp4* was not expressed in *Adamts9* mutants, similar to that observed in the *Pofut2* knockout (Fig. 1G). (F) *Brachyury (T)* was expressed in a truncated domain in 1/5 *Adamts9* mutants, but was absent in 4/5 embryos. (G) *Snail* was expressed weakly in 1/3 *Adamts9* mutants. Embryos are oriented proximal up and distal down. Wild-type embryos are oriented anterior to the left and posterior to the right. The anterior posterior orientation of *Pofut2* mutants is not known.

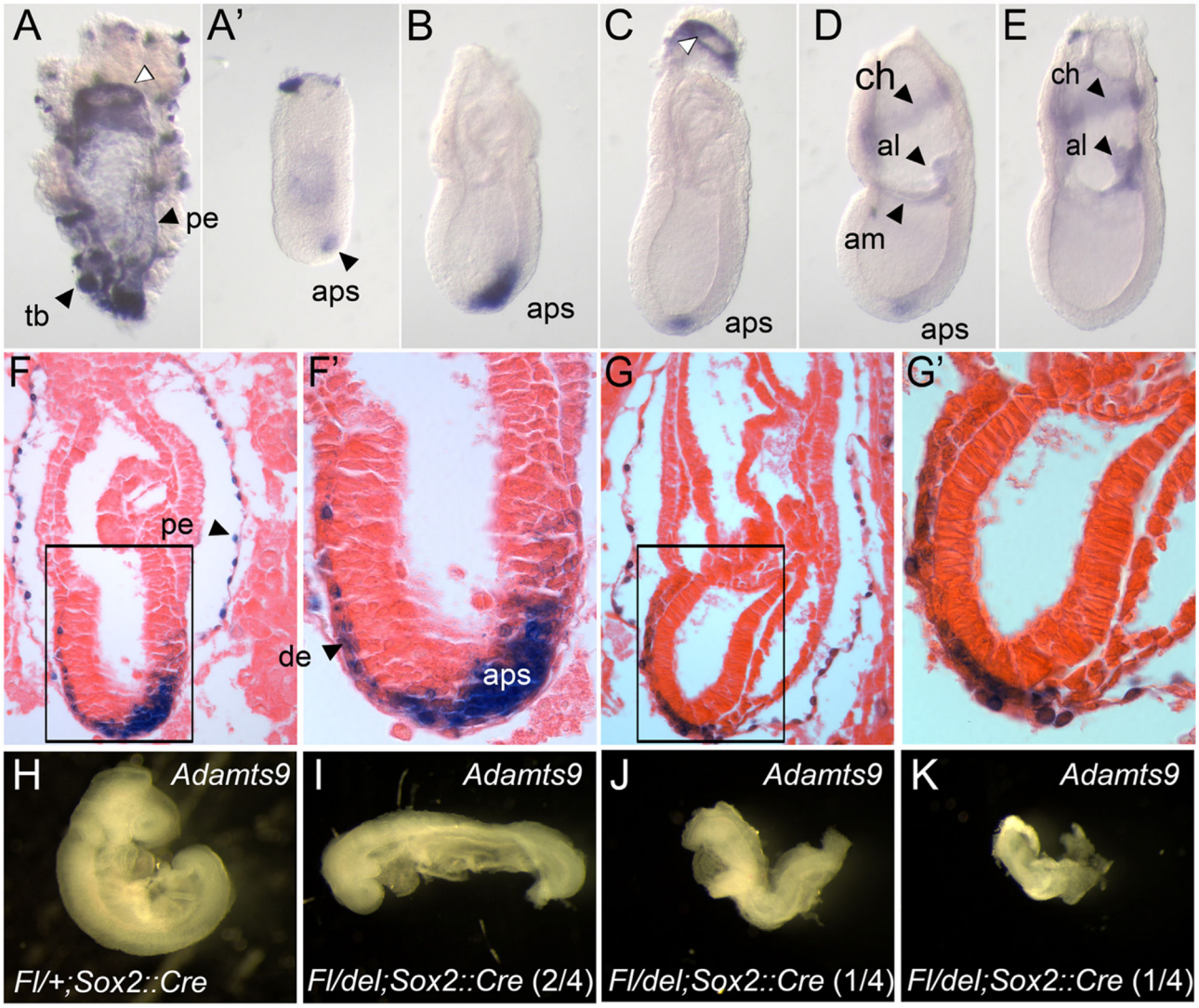

Fig. 5.

Adamts9 is expressed dynamically during gastrulation, in distinct extraembryonic and embryonic tissues. (A–E) Whole mount *in situ* hybridization analysis of *Adamts9* expression at E 7.5. *Adamts9* mRNA was detected in extraembryonic mesoderm of the amnion, allantois, and chorion, and in the parietal endoderm cells (pe), trophoblast giant cells, ring of proximal visceral endoderm adjacent to the ectoplacental cone (white arrowhead), and in the anterior primitive streak. (A′) Trophoblast and parietal endoderm was removed from embryo shown in A. (F–G′) E 6.5 (F, F′) and E 7.5 (G, G′) $Adamts9^{lacZ/+}$ embryos were stained for β-galactosidase activity, then sectioned and stained with eosin. β-gal activity was detected in the anterior primitive streak, parietal endoderm, and definitive endoderm. β-gal activity in the definitive endoderm, likely reflects perdurance of β-gal activity in cells originating from the anterior primitive streak. (H–K) Evaluating the effect of *Adamts9* deletion in the epiblast at E9.5. (H) Wild-type *Adamts9* embryos (*Fl/+*;Sox2::Cre) had turned, the neural tube was closed, heart was developing, and somites were visible. (I–K) In contrast, *Adamts9* epiblast mutants (*Fl/del;Sox2::Cre*) embryos failed to turn (4/4) and were considerably delayed. Two

of the four *Adamts9* epiblast mutants (J and K) had a severely truncated and kinked axis similar to that observed in *Pofut2* epiblast mutants. Embryos are oriented proximal up and distal down. Wild-type embryos are oriented anterior to the left; anterior posterior orientation of *Adamts9* mutants is not known. Anterior primitive streak (aps), amnion (am), allantois (al), chorion (ch), definitive endoderm (de), parietal endoderm (pe), trophoblast (tb).

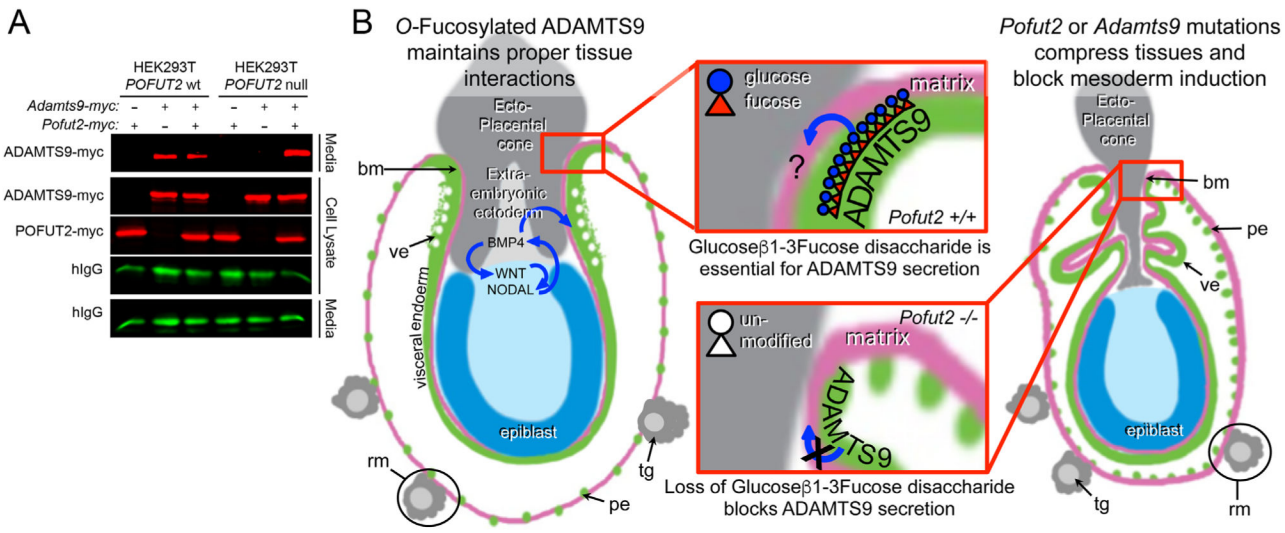

Fig. 6.

Loss of *POFUT2* blocks secretion of ADAMTS9 in HEK293T cells.(A) Western blot analysis of myc-tagged ADAMTS9-N-L2 (ADAMTS9-myc) secretion from wild-type HEK293T cells or *Pofut2* CRISPR/Cas9-targeted HEK293T cells (HEK293T *Pofut2* null). Cells were co-transfected with expression plasmids encoding *Adamts9-myc* and *hIgG* with or without additional *Pofut2-myc* or empty vector. In HEK293T cells, ADAMTS9 is secreted into the media with or without transfected *Pofut2-myc*. In contrast, in CRISPR/Cas9-mutated HEK293T cells ADAMTS9, although observed in the cell lysate, fails to be secreted into the medium. Co-transfection with *Pofut2-myc* rescues secretion defects in HEK293T *Pofut2* null cells. (B) Model for action of POFUT2 and ADAMTS9 in the early gastrula. We propose that *O*-fucosylation of ADAMTS9 promotes the proper arrangement of extraembryonic tissues (grey and green) critical for specification of visceral endoderm characteristics (green) and maintaining signals essential for mesoderm induction in the epiblast (blue). We hypothesize that one possible function of ADAMTS9 is to act locally (red square) to anchor proximal visceral endoderm cells to the ECM or ectoplacental cone cells. We predict that loss of *Pofut2* (by blocking secretion of ADAMTS9) or loss of *Adamts9* disrupts this anchor point causing the visceral/parietal endoderm layers to slip. This disturbance alters the properties of the extraembryonic ectoderm or displaces the tissue. As a consequence, the visceral endoderm does not receive BMP signals essential for maintaining characteristics such as apical vacuoles (white spots) and the epiblast is unable to maintain signals needed for mesoderm induction (WNT and NODAL). The increased laminin staining in Reichert's membrane (pink) in *Pofut2* mutants (Du et al., 2010) could result from loss of this anchor point (retraction of the membrane), or alternatively from loss of ADAMTS9 function in the parietal endoderm cells or trophoblast giant cells. Wild-type and mutant embryos are oriented proximal up and distal down. Abbreviations: ectoplacental cone (ec), epiblast (ep), parietal endoderm (pe), Reichert's membrane (rm), trophoblast giant cells (tg), visceral endoderm (ve).